Journal of Solid State Chemistry **155,** 433–440 (2000)
doi:10.1006/jssc.2000.8946, available online at http://www.idealibrary.com on IDEAL®

Accidental Silicon-Containing Compounds: Crystal Structures of $La_3Al_{0.44}Si_{0.93}S_7$, $BaSm_4(SiO_4)_3Se$, and Monoclinic and Orthorhombic $Ln_2(SiO_4)Te$ (Ln = Nd and Sm)

Yuting Yang and James A. Ibers[1]

Department of Chemistry, Northwestern University, 2145 Sheridan Road, Evanston, Illinois 60208-3113

Received June 15, 2000; in revised form July 31, 2000; accepted August 17, 2000; published online November 29, 2000

The compounds $La_3Al_{0.44}Si_{0.93}S_7$, $BaSm_4(SiO_4)_3Se$, and monoclinic and orthorhombic $Ln_2(SiO_4)Te$ (Ln = Nd and Sm) were obtained accidentally by reactions in fused-silica tubes. $La_3Al_{0.44}Si_{0.93}S_7$ crystallizes in the hexagonal space group $P6_3$ with two formula units in a cell of dimensions $a = 10.277(2)$, $c = 5.793(1)$ Å ($T = 153$ K). The structure consists of chains of face-sharing AlS_6 octahedra and isolated SiS_4 tetrahedra. The LaS_8 coordination polyhedron is a square antiprism. $BaSm_4(SiO_4)_3Se$ crystallizes in the hexagonal space group $P6_3/m$ with two formula units in a cell of dimensions $a = 9.869(1)$, $c = 6.851(1)$ Å ($T = 153$ K). The structure is formed by orthosilicate ($[SiO_4]^{4-}$) tetrahedra separated by Ba^{2+} and Sm^{3+} cations. The Ba^{2+} and $Sm(1)^{3+}$ cations are disordered in an MS_9 tricapped trigonal prism and the $Sm(2)^{3+}$ cation is in a monocapped trigonal prism. Monoclinic ($P2_1/c$) $Ln_2(SiO_4)Te$ (Ln = Nd and Sm) is a layered structure with four formula units in a cell of dimensions $a = 9.823(2)$, $b = 6.421(1)$, $c = 8.676(2)$ Å, $\beta = 94.60(3)^\circ$ ($T = 153$ K) for Ln = Nd, and $a = 9.760(2)$, $b = 6.357(1)$, $c = 8.601(2)$ Å, $\beta = 94.87(3)^\circ$ ($T = 153$ K) for Ln = Sm. The layer is formed by $[SiO_4]^{4-}$ tetrahedra separated by Ln and Te atoms. The $Ln(1)O_7Te$ polyhedron is a square antiprism and the $Ln(2)O_4Te_4$ polyhedron is a bicapped trigonal prism. Orthorhombic $Pbcm$ $Ln_2(SiO_4)Te$ (Ln = Nd and Sm) is a layered structure with four formula units in a cell of dimensions $a = 6.279(1)$, $b = 7.189(1)$, $c = 11.168(2)$ Å ($T = 153$ K) for Ln = Nd, and $a = 6.201(1)$, $b = 7.091(1)$, $c = 11.077(2)$ Å ($T = 115$ K) for Ln = Sm. The layer is formed by $[SiO_4]^{4-}$ tetrahedra separated by Ln and Te atoms. The $Ln(1)O_6Te_3$ polyhedron is a tricapped trigonal prism; the $Ln(2)O_6Te_2$ polyhedron is a dodecahedron. Orthorhombic $Ln_2(SiO_4)Te$, $\rho = 6.696$ g/cm^3 for Ln = Nd and $\rho = 7.096$ g/cm^3 for Ln = Sm, are denser than the monoclinic forms, $\rho = 6.188$ g/cm^3 for Ln = Nd and $\rho = 6.500$ g/cm^3 for Ln = Sm. © 2000 Academic Press

[1] To whom correspondence should be addressed. E-mail: ibers@chem.northwestern.edu.

INTRODUCTION

Rare-earth elements are highly reactive at elevated temperatures. If reactions involving these elements are carried out in unprotected fused-silica tubes, then various silicon-containing compounds, of higher stability than possible target compounds, can be formed (1–4). Here we report the structures of five new rare-earth silicates and one silicon compound that were formed during our exploration of potential new rare-earth chalcogenides.

EXPERIMENTAL

Syntheses

All reactions were carried out at 1123 or 1173 K for 7 days in unprotected fused-silica tubes with the use of a $BaBr_2$/KBr eutectic flux (molar ratio 1.1:1). Approximate compositions of the products were obtained with EDX measurements on a Hitachi *S*-4500 scanning electron microscope; final compositions were established from the single-crystal X-ray structure determinations.

$La_3Al_{0.44}Si_{0.93}S_7$. A few brown needles were obtained in the reaction of BaS (Alfa Aesar, 99.7%), La (Alfa Aesar, 99.9%), Al (Aesar, 99.8%), and S (Alfa Aesar, 99.7%) in the ratio of 1:1:1:3. The main products were La/S phases, as detected by EDX measurements. Such measurements on the needles confirmed the presence of La, Al, Si, and S in the ratio 6:1:2:14. $La_3Al_{0.44}Si_{0.93}S_7$ can also be obtained through direct synthesis from La, Al, Si, and S at the same temperature.

$BaSm_4(SiO_4)_3Se$. Yellow needles were obtained in a reaction of BaSe (Alfa Aesar, 99.5%), Ag (Alfa Aesar, 99.9%), Sm (Alfa Aesar, 99.9%), and Se (Aldrich, 99.5%) in a ratio of 2:3:1:3. The yield was about 30%. EDX measurements confirmed the presence of Ba, Sm, Si, and Se in the ratio 1:4:3:1.

$Ln_2(SiO_4)Te$ (Ln = Nd and Sm). Two types of crystals, light purple prismatic needles (orthorhombic) and yellow

0022-4596/00 $35.00

flat needles (monoclinic) for Ln = Nd and dark red prisms (orthorhombic) and vivid red flat needles (monoclinic) for Ln = Sm, were obtained in a yield of about 20% in the reaction of BaTe (Alfa Aesar, 99.5%), Nd (Alfa Aesar, 99.9%) or Sm (Alfa Aesar, 99.9%), Zn (Johnson Mathey, 99.999%), and Te (Aldrich, 99.8%) in the ratio of 1:1:1:3. EDX analysis of both types of crystals confirmed the presence of *Ln*, Si, Te, and O with *Ln*, Si, Te = 2:1:1. Orthorhombic $Sm_2(SiO_4)Te$ was characterized previously as a byproduct in the vapor transport of $SmTe_2$ with I_2 in a fused-silica ampoule (4).

Crystallography

Diffraction data from a prismatic single crystal of $Sm_2(SiO_4)Te$ were collected at 115 K on a Picker automatic four-circle diffractometer (5). Forty peaks in the 2θ range 30–35° were used to obtain the unit cell. Data for all the other compounds were collected at 153 K on a Bruker SMART-1000 CCD diffractometer (6) with exposure times of 15 or 25 s/frame and with a step of 0.25° or 0.3° in ω. Face-indexed absorption corrections (7) were applied to all data sets. The CCD data were further corrected for frame variations with the use of the program SADABS (6). Solutions were found with the use of the direct methods program SHELXS (7). Each structure was refined by full-matrix least-squares methods with the program SHELXL (7). The final structures were examined with the use of MISSYM (8); no additional symmetries were found. The refined cell parameters and other relevant crystal data are given in Table 1 and the final positional parameters and equivalent isotropic displacement parameters are given in Table 2.

$La_3Al_{0.44}Si_{0.93}S_7$. This compound belongs to the well-known $Ln_3MM'Q_7$ structure type (9), which is adopted by a large number of compounds (10, 11). The M site is octahedral and the M' site is tetrahedral. In the present compound Al was assigned to the M site and Si to the M' site; these lead to Al–S bond lengths of 2.582(7) and 2.590(7) Å, to be compared with 2.431(1)–2.443(1) Å in $MgAl_2S_4$ (12) for octahedral Al, and to Si–S bond lengths of 2.110(4) and 2.166(2) Å, to be compared with 2.133(1) Å in SiS_2 (13) and 2.089(4)–2.136(2) Å in $La_6MgSi_2S_{14}$ (14). The occupancies of Al and Si refined to 0.44(1) and 0.93(1), respectively. The resultant charge on the compound is balanced. Metrical data are presented in Table 3.

$BaSm_4(SiO_4)_3Se$. A solution was found in space group $P6_3/m$. There are two possible sites (Wyckoff positions 4*f* and 6*h*) for the Ba^{2+} and Sm^{3+} cations. A refinement in which both were placed at the 4*f* site led to an occupancy of 54% Ba^{2+} and 46% Sm^{3+}, whereas a refinement in which they were both assigned to the 6*h* site led to a 9% occupancy

TABLE 1
Crystal Data and Structure Refinements

Empirical formula	$La_3Al_{0.44}Si_{0.93}S_7$	$BaSm_4(SiO_4)_3Se$	Monoclinic $Nd_2(SiO_4)Te$	Monoclinic $Sm_2(SiO_4)Te$	Orthorhombic $Nd_2(SiO_4)Te$	Orthorhombic $Sm_2(SiO_4)Te$
Formula weight	679.14	1093.97	508.17	520.39	508.17	520.39
Space group	$P6_3$	$P6_3/m$	$P2_1/c$	$P2_1/c$	*Pbcm*	*Pbcm*
a (Å)[a]	10.277(2)	9.869(1)	9.823(2)	9.760(2)	6.279(1)	6.201(1)
b (Å)	10.277(2)	9.869(1)	6.421(1)	6.357(1)	7.189(1)	7.091(1)
c (Å)	5.793(1)	6.851(1)	8.676(2)	8.601(2)	11.168(2)	11.077(2)
α (°)	90	90	90	90	90	90
β (°)	90	90	94.60(3)	94.87(3)	90	90
γ (°)	120	120	90	90	90	90
Volume (Å^3)	529.9(2)	577.9(2)	545.5(2)	531.7(2)	504.1(2)	487.1(2)
Z	2	2	4	4	4	4
ρ_c (g/cm^3)	4.256	6.287	6.188	6.500	6.696	7.096
μ (cm^{-1})	133.28	268.84	241.99	273.82	261.87	298.91
Transmission factors	0.36–0.71	0.18–0.54	0.30–0.84	0.22–0.85	0.17–0.45	0.36–0.48
θ range (deg)	2.29–28.46	2.38–28.66	2.08–28.46	2.09–28.37	3.24–28.56	3.29–30.56
Reflections collected/unique	4728/861	5169/514	3786/1276	3054/1230	4160/648	4918/784
R(int)	0.0258	0.0330	0.0309	0.0285	0.0323	0.0570
Goodness-of-fit	1.021	1.229	0.869	1.016	1.430	0.923
Residual electron density	− 1.0(2) to 2.7(2)	− 1.2(3) to 2.1(3)	− 1.5(4) to 1.7(4)	− 1.6(4) to 2.4(4)	− 2.6(6) to 4.2(6)	− 1.9(4) to 1.4(4)
R_1[b] [$I > 2\sigma(I)$]	0.0258	0.0223	0.0253	0.0274	0.0291	0.0212
wR_2[c] (all data)	0.0566	0.0638	0.0602	0.0664	0.0732	0.0550

[a] All data were collected at 153 K except those of orthorhombic $Sm_2(SiO_4)Te$, which were collected at 115 K.
[b] $R_1 = \sum||F_o| - |F_c||/|F_o|$.
[c] $wR_2 = \{\sum[w(F_o^2 - F_c^2)^2]/\sum wF_o^4\}^{1/2}$; $w^{-1} = \sigma^2(F_o^2) + (0.04F_o^2)^2$ for $F_o^2 \geq 0$ and $w^{-1} = \sigma^2(F_o^2)$ for $F_o^2 < 0$.

TABLE 2
Atomic Coordinates and Equivalent Isotropic Displacement Parameters (Å^2) of $La_3Al_{0.44}Si_{0.93}S_7$, $BaSm_4(SiO_4)_3Se$, and Monoclinic and Orthorhombic $Ln_2(SiO_4)Te$ (Ln = Nd and Sm)

Atom	x	y	z	U(eq)[a]	Wyckoff position	Atom	x	y	z	U(eq)	Wyckoff position
		$La_3Al_{0.44}Si_{0.93}S_7$						$BaSm_4(SiO_4)_3Se$			
La(1)	− 0.36091(3)	− 0.23336(3)	− 0.2842(1)	0.0107(1)	6*c*	Sm(1)	0.6667	0.3333	0.00341(8)	0.0138(2)	4*f*
S(1)	− 0.0832(1)	− 0.2372(2)	− 0.2705(4)	0.0174(3)	6*c*	Ba(1)	0.6667	0.3333	0.00341(8)	0.0138(2)	4*f*
S(2)	− 0.5234(2)	− 0.1111(2)	− 0.0055(2)	0.0112(3)	6*c*	Sm(2)	0.24833(4)	0.25535(4)	0.2500	0.0135(2)	6*h*
S(3)	− 0.3333	− 0.6667	− 0.0002(5)	0.0120(5)	2*b*	Se(1)	0	0	0	0.0221(3)	2*b*
Si(1)	− 0.3333	− 0.6667	− 0.3644(6)	0.0067(9)	2*b*	Si(1)	0.0339(2)	0.4152(2)	0.2500	0.0109(4)	6*h*
Al(1)	0.00	0.00	− 0.022(2)	0.011(2)	2*a*	O(1)	0.0955(5)	0.3656(6)	0.0590(7)	0.030(1)	12*i*
						O(2)	0.1361(6)	0.6079(6)	0.2500	0.017(1)	6*h*
						O(3)	0.5053(7)	0.1528(6)	0.2500	0.023(1)	6*h*
		$Nd_2(SiO_4)Te$ ($P2_1/c$)						$Sm_2(SiO_4)Te$ ($P2_1/c$)			
Nd(1)	0.10634(4)	0.65256(6)	0.19324(5)	0.0063(1)	4*e*	Sm(1)	0.10831(4)	0.65375(6)	0.19395(5)	0.0069(1)	4*e*
Nd(2)	0.34851(4)	0.19635(6)	0.33540(5)	0.0063(1)	4*e*	Sm(2)	0.34770(4)	0.19713(6)	0.33507(5)	0.0069(1)	4*e*
Te(1)	0.59479(5)	0.21409(7)	0.11322(6)	0.0075(1)	4*e*	Te(1)	0.59190(6)	0.21529(8)	0.11461(6)	0.0076(2)	4*e*
Si(1)	0.1263(2)	0.1896(3)	0.0564(2)	0.0060(4)	4*e*	Si(1)	0.1256(2)	0.1903(3)	0.0565(3)	0.0060(4)	4*e*
O(1)	0.0186(5)	0.8077(7)	0.4215(6)	0.005(1)	4*e*	O(1)	0.0213(6)	0.8053(8)	0.4227(7)	0.007(1)	4*e*
O(2)	0.1263(5)	0.3674(8)	0.3753(6)	0.006(1)	4*e*	O(2)	0.1257(6)	0.3672(8)	0.3724(7)	0.008(1)	4*e*
O(3)	0.1555(5)	0.0118(8)	0.1849(6)	0.009(1)	4*e*	O(3)	0.1562(6)	0.0088(8)	0.1840(6)	0.008(1)	4*e*
O(4)	0.2498(5)	0.3585(8)	0.0905(6)	0.008(1)	4*e*	O(4)	0.2493(6)	0.3648(8)	0.0896(6)	0.008(1)	4*e*
		$Nd_2(SiO_4)Te$ (*Pbcm*)						$Sm_2(SiO_4)Te$ (*Pbcm*)			
Nd(1)	0.11273(6)	0.03793(6)	0.2500	0.0066(2)	4*d*	Sm(1)	0.11269(6)	0.03591(5)	0.2500	0.0034(1)	4*d*
Nd(2)	0.61056(6)	0.2500	0	0.0075(2)	4*c*	Sm(2)	0.61065(6)	0.2500	0	0.0043(1)	4*c*
Te(1)	0.40250(8)	0.42169(9)	0.2500	0.0093(2)	4*d*	Te(1)	0.40356(8)	0.41621(7)	0.2500	0.0049(1)	4*d*
Si(1)	0.1128(3)	0.2500	0	0.0059(5)	4*c*	Si(1)	0.1129(3)	0.2500	0	0.0030(4)	4*c*
O(1)	0.0497(6)	0.7684(5)	0.1154(3)	0.0079(7)	8*e*	O(1)	0.0503(6)	0.7671(5)	0.1161(3)	0.0040(7)	8*e*
O(2)	0.2684(7)	0.0763(5)	0.0348(3)	0.0077(7)	8*e*	O(2)	0.2700(6)	0.0747(5)	0.0347(3)	0.0047(7)	8*e*

[a] U(eq) is defined as one-third of the trace of the orthogonalized U_{ij} tensor.

by Ba^{2+}. In the final refinement, charge balance was achieved by the assignments of Ba^{2+} and Sm^{3+} each at 50% occupancy to the 4*f* site and Sm^{3+} at full occupancy to the 6*h* site. Metrical data are presented in Table 4.

TABLE 3
Bond Lengths (Å) and Selected Bond Angles (°) for $La_3Al_{0.44}Si_{0.93}S_7$

Bond length (Å)		Bond angle (°)	
La(1)–S(1)	2.863(1)	S(3)–Si(1)–S(2) × 3	112.17(8)
La(1)–S(1)	2.875(1)	S(2)–Si(1)–S(2) × 3	106.64(9)
La(1)–S(2)	2.908(2)	S(1)–Al(1)–S(1) × 3	91.9(3)
La(1)–S(2)	3.013(2)	S(1)–Al(1)–S(1) × 3	179.8(5)
La(1)–S(1)	3.030(2)	S(1)–Al(1)–S(1) × 6	88.31(3)
La(1)–S(2)	3.039(2)	S(1)–Al(1)–S(1) × 3	91.5(3)
La(1)–S(3)	3.044(1)		
La(1)–S(1)	3.178(2)		
Si(1)–S(3)	2.110(4)		
Si(1)–S(2) × 3	2.166(2)		
Al(1)–S(1) × 3	2.582(7)		
Al(1)–S(1) × 3	2.590(7)		

Monoclinic and orthorhombic $Ln_2(SiO_4)Te$ (Ln = Nd and Sm). Solution and refinements of these structures were straightforward and require no additional comments.

RESULTS AND DISCUSSION

$La_3Al_{0.44}Si_{0.93}S_7$

The structure of $La_3Al_{0.44}Si_{0.93}S_7$ belongs to $Ln_3MM'Q_7$ structure type (9), where Ln is a rare-earth element, M

TABLE 4
Bond Lengths (Å) and Selected Bond Angles (°) for $BaSm_4(SiO_4)_3Se$

Bond length (Å)				Bond angle (°)	
Sm(1)–O(3) × 3	2.393(4)	Sm(2)–O(1) × 2	2.382(4)	O(1)–Si(1)–O(1)	107.9(4)
Sm(1)–O(2) × 3	2.451(4)	Sm(2)–O(1) × 2	2.610(5)	O(1)–Si(1)–O(3) × 2	114.3(2)
Sm(1)–O(1) × 3	2.747(5)	Sm(2)–Se(1) × 2	3.0190(5)	O(1)–Si(1)–O(2) × 2	104.1(2)
Ba(1)–O(3) × 3	2.393(4)	Si(1)–O(1) × 2	1.618(5)	O(3)–Si(1)–O(2)	111.3(3)
Ba(1)–O(2) × 3	2.451(4)	Si(1)–O(3)	1.624(6)		
Ba(1)–O(1) × 3	2.747(5)	Si(1)–O(2)	1.648(5)		
Sm(2)–O(2)	2.334(5)				

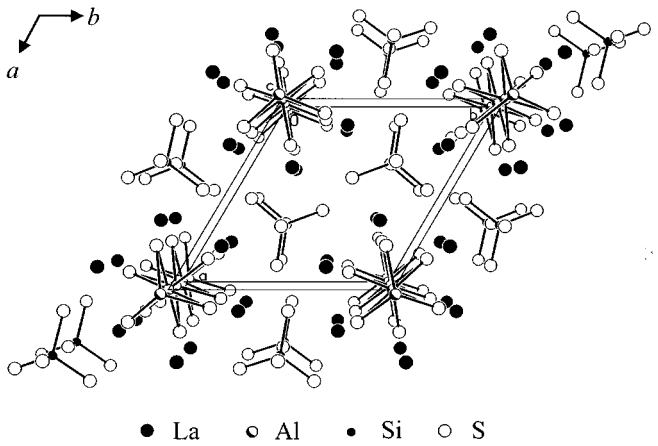

FIG. 1. View down [001] of the structure of $La_3Al_{0.44}Si_{0.93}S_7$.

and M' are metals, and Q is a chalcogen. Its structure is shown in Figs. 1 and 2. It may be considered a one-dimensional structure with face-sharing chains of AlS_6 octahedra and isolated SiS_4 tetrahedra extending in the c direction. The LaS_8 polyhedron shown in Fig. 3 is a square antiprism. The La–S distances range from 2.863(1) to 3.178(2) Å, close to those of 2.877(1)–3.108(2) Å in $La_6MgSi_2S_{14}$ (14). The Si–S and Al–S distances are reasonable, as discussed above.

$BaSm_4(SiO_4)_3Se$

The structure of $BaSm_4(SiO_4)_3Se$ is shown in Fig. 4. $BaSm_4(SiO_4)_3Se$ has the apatite $Ca_5(PO_4)_3F$ type of structure (15). The apatite structure is very common, some examples being $Ba_3LaNa(PO_4)_3F$ (16), $MLn_9(SiO_4)_6O_2$ (M = alkali metal) (17), and $NaPr_9(SiO_4)_6S_2$ (18). Note that the large cations can be alkali metals, alkaline earths, rare earths (19–22), and even smaller transition metals (such as Mn(23)). In the present structure two orthosilicate ($[SiO_4]^{4-}$) tetrahedra point up and down forming a pair that extends into chains along c. Oxygen atoms of these tetrahedra are separated by Ba^{2+} and Sm^{3+} cations and form the hexagonal framework of the structure. There are two crystallographically distinct sites for these cations. In the 4*f* site, which contains 50% Ba^{2+} and 50% Sm^{3+}, these ions are coordinated by nine O atoms in a tricapped trigonal prism (Fig. 5) with three long bonds, 2.747(5) × 3 Å, and

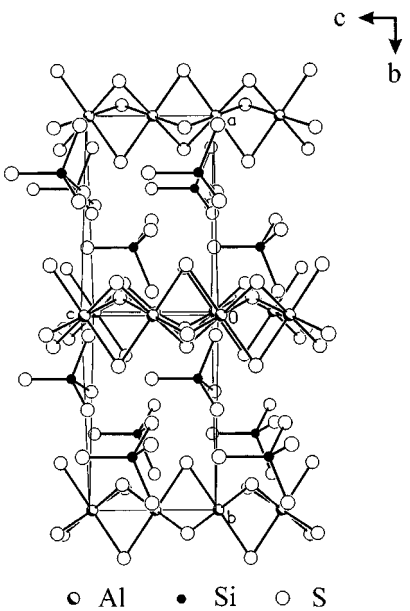

FIG. 2. Structure of $La_3Al_{0.44}Si_{0.93}S_7$ in the *bc* plane. The La atoms have been removed for the sake of clarity.

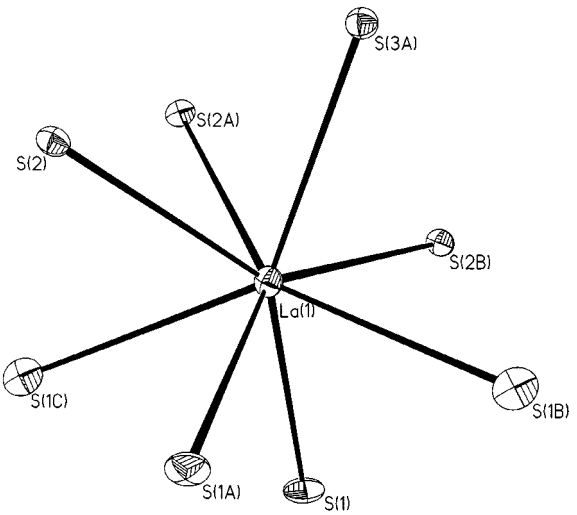

FIG. 3. Square antiprismatic coordination about the La center in $La_3Al_{0.44}Si_{0.93}S_7$; atoms S(1A), S(1B), S(2), and S(3A) are on the top, and the others are on the bottom.

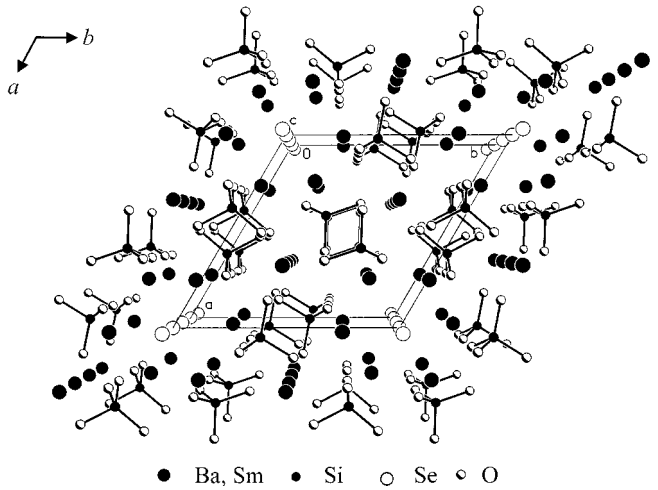

FIG. 4. View of the structure of $BaSm_4(SiO_4)_3Se$ in the *ab* plane.

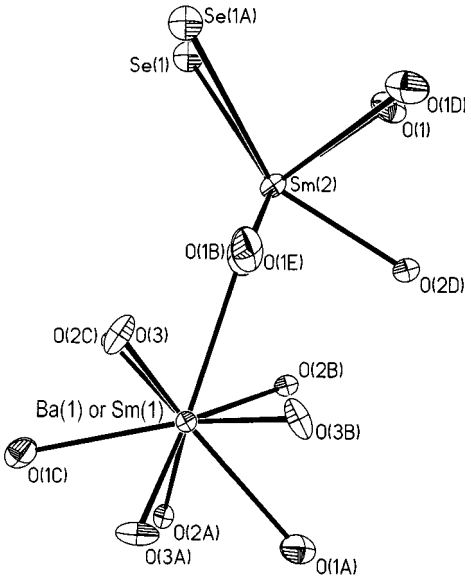

FIG. 5. Coordination of Sm on the 4*f* and 6*h* sites of $BaSm_4(SiO_4)_3Se$.

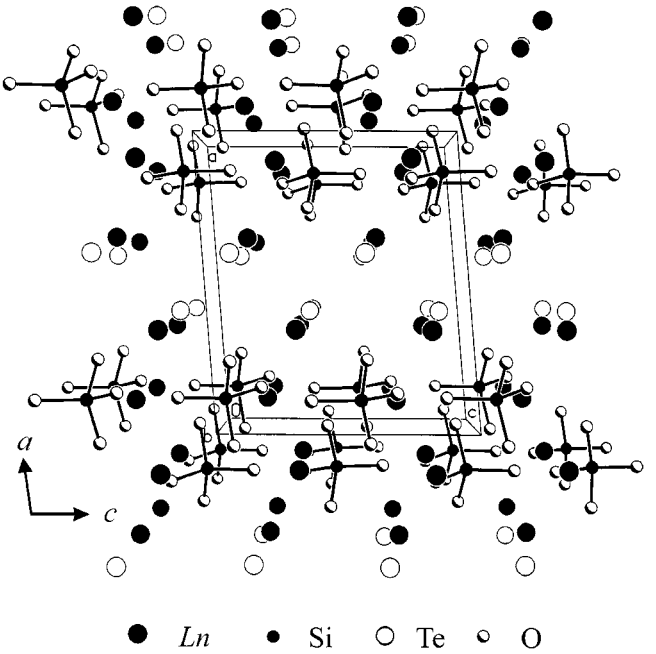

FIG. 6. Structure of monoclinic $Ln_2(SiO_4)Te$ (Ln = Nd and Sm) as viewed down [010].

six shorter ones, 2.393(4) × 3 and 2.451(4) × 3 Å (Table 4). The Sm^{3+} cation on the 6*h* site is coordinated both by O and Se atoms as a SmO_5Se_2 monocapped trigonal prism (Fig. 5). The Sm–Se distance is 3.0190(5) Å and the Sm–O distances range from 2.334(5) to 2.610(5) Å; compare these with the Sm–Se distances of 2.945(1)–3.079(1) Å and Sm–O distances of 2.432(3)–2.553(3) Å in $Sm_2(SiO_4)Se$ (4). Coordination of a Ln^{3+} cation by both O and S or Se atoms is common, for example in $LaCrOS_2$ (24) and $La_5V_3O_7S_6$ (25).

Dimorphism in $Ln_2(SiO_4)Te$

In addition to the monoclinic and orthorhombic $Ln_2(SiO_4)Te$ (Ln = Nd and Sm) phases of the present work, the monoclinic and orthorhombic $Pr_2(SiO_4)Te$ phases are known (26), as is orthorhombic $Sm_2(SiO_4)Te$ (4). The monoclinic $Ln_2(SiO_4)Te$ (Ln = Nd and Sm) phases are not isostructural with $Pr_2(SiO_4)Te$, whereas the orthorhombic phases are. Although the reactions involved in the formation of these compounds are very different, the Nd and Sm compounds being formed accidentally in unprotected fused-silica tubes as detailed above and the Pr compounds being formed at 1173 K from Pr, TeO_2, and SiO_2 in a CsCl flux in fused-silica tubes, in each instance the monoclinic and orthorhombic phases formed together. The orthorhombic phase is the denser: 6.696 vs 6.188 g/cm^3 for the Nd

TABLE 5
Bond Lengths (Å) and Selected Bond Angles (°) for Monoclinic $Ln_2(SiO_4)Te$ (Ln = Nd and Sm)

	$Nd_2(SiO_4)Te$				$Sm_2(SiO_4)Te$		
Nd(1)–O(3)	2.359(5)	Nd(2)–Te(1)	3.214(1)	Sm(1)–O(3)	2.308(5)	Sm(2)–Te(1)	3.171(1)
Nd(1)–O(2)	2.416(5)	Nd(2)–Te(1)	3.325(1)	Sm(1)–O(2)	2.379(5)	Sm(2)–Te(1)	3.286(1)
Nd(1)–O(1)	2.435(5)	Nd(2)–Te(1)	3.3942(9)	Sm(1)–O(1)	2.409(6)	Sm(2)–Te(1)	3.3678(9)
Nd(1)–O(1)	2.458(5)	Si(1)–O(3)	1.605(5)	Sm(1)–O(1)	2.429(6)	Si(1)–O(3)	1.603(5)
Nd(1)–O(4)	2.559(5)	Si(1)–O(2)	1.613(6)	Sm(1)–O(4)	2.506(6)	Si(1)–O(2)	1.625(6)
Nd(1)–O(1)	2.684(5)	Si(1)–O(1)	1.638(6)	Sm(1)–O(2)	2.676(6)	Si(1)–O(1)	1.632(6)
Nd(1)–O(2)	2.694(5)	Si(1)–O(4)	1.636(5)	Sm(1)–O(1)	2.701(5)	Si(1)–O(4)	1.647(6)
Nd(1)–Te(1)	3.287(1)	O(3)–Si(1)–O(2)	120.1(3)	Sm(1)–Te(1)	3.257(1)	O(3)–Si(1)–O(2)	119.3(3)
Nd(2)–O(2)	2.493(5)	O(3)–Si(1)–O(1)	110.9(3)	Sm(2)–O(2)	2.467(6)	O(3)–Si(1)–O(1)	111.2(3)
Nd(2)–O(4)	2.492(5)	O(2)–Si(1)–O(1)	106.7(3)	Sm(2)–O(4)	2.484(5)	O(2)–Si(1)–O(1)	106.3(3)
Nd(2)–O(3)	2.512(5)	O(3)–Si(1)–O(4)	104.9(3)	Sm(2)–O(3)	2.490(6)	O(3)–Si(1)–O(4)	106.0(3)
Nd(2)–O(4)	2.511(5)	O(2)–Si(1)–O(4)	105.6(3)	Sm(2)–O(4)	2.496(6)	O(2)–Si(1)–O(4)	105.0(3)
Nd(2)–Te(1)	3.1715(9)	O(1)–Si(1)–O(4)	108.1(3)	Sm(2)–Te(1)	3.1424(9)	O(1)–Si(1)–O(4)	108.5(3)

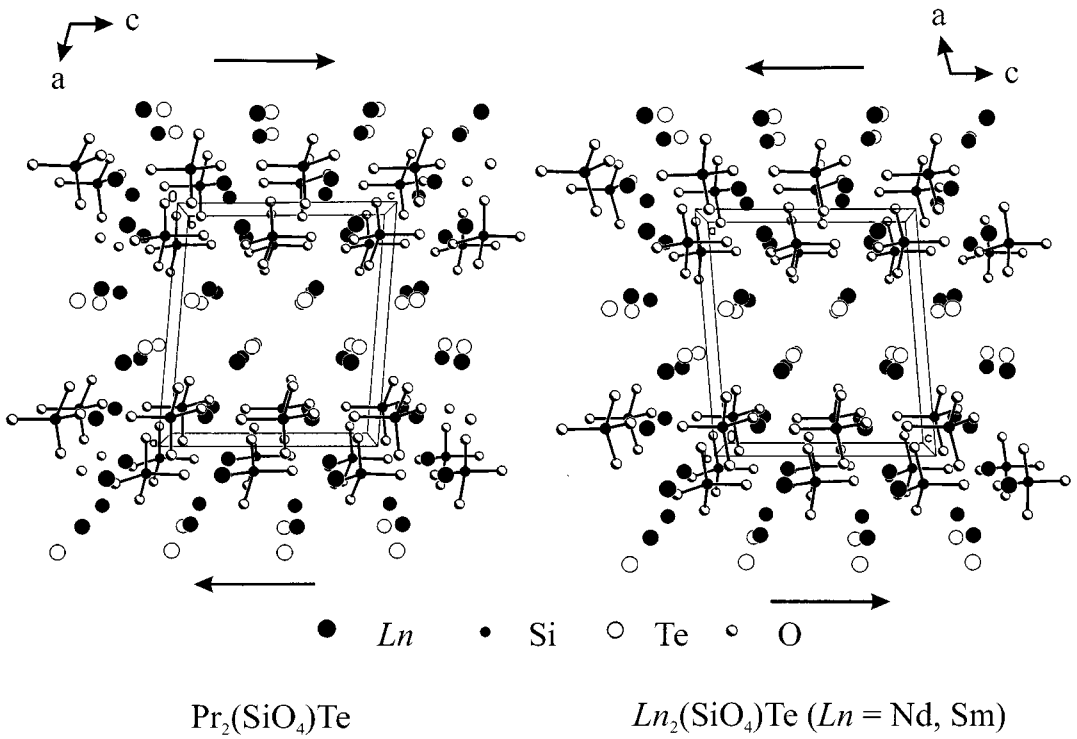

FIG. 7. Comparison of the structures of monoclinic $Ln_2(SiO_4)Te$ (Ln = Nd and Sm) and monoclinic $Pr_2(SiO_4)Te$.

compound, 7.096 vs 6.500 g/cm^3 for the Sm compound, and 6.45 vs 5.98 g/cm^3 for the Pr compound (26). However, the earlier preparation of $Sm_2(SiO_4)Te$ (4), which involved a chemical transport experiment of $SmTe_2$ with I_2 in fused-silica tubes, apparently afforded only the orthorhombic phase.

Monoclinic $Ln_2(SiO_4)Te$ (Ln = Nd and Sm)

These compounds are isostructural. Their layered structure is shown in Fig. 6. The layer is formed by $[SiO_4]^{4-}$ tetrahedra separated by *Ln* and Te atoms. *Ln* atoms occupy two crystallographic sites: atom *Ln*(1), located within the layer, is coordinated by seven O atoms and one Te atom in a square antiprism, and atom *Ln*(2), located between the layers, is coordinated by four O and four Te atoms in a bicapped trigonal prism. Metrical data are presented in Table 5. The Sm–O distances range from 2.308(5) to 2.701(5) Å; the Sm–Te distances range from 3.1424(9) to 3.3678(9) Å; the Nd–O distances range from 2.359(5) to 2.694(5) Å; and the Nd–Te distances range from 3.1715(9) to 3.3942(9) Å. Figure 7 compares this structure with that of

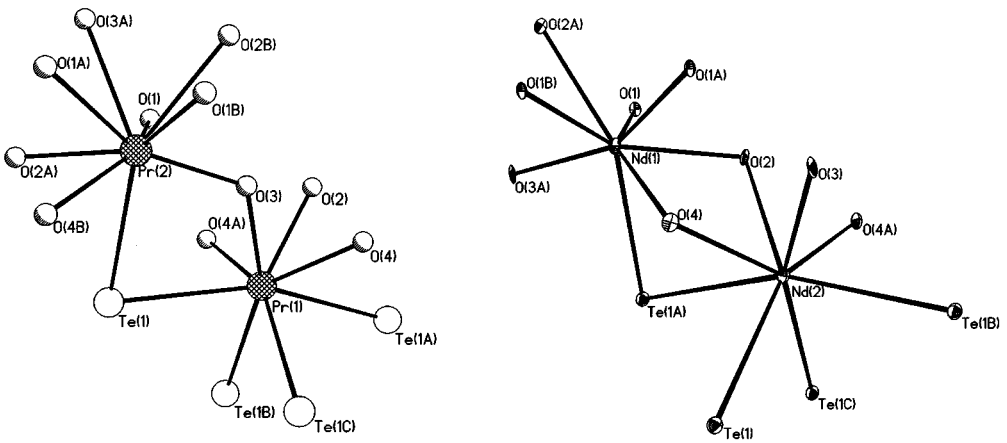

FIG. 8. Rare-earth coordination in monoclinic $Ln_2(SiO_4)Te$ (Ln = Nd and Sm) and monoclinic $Pr_2(SiO_4)Te$.

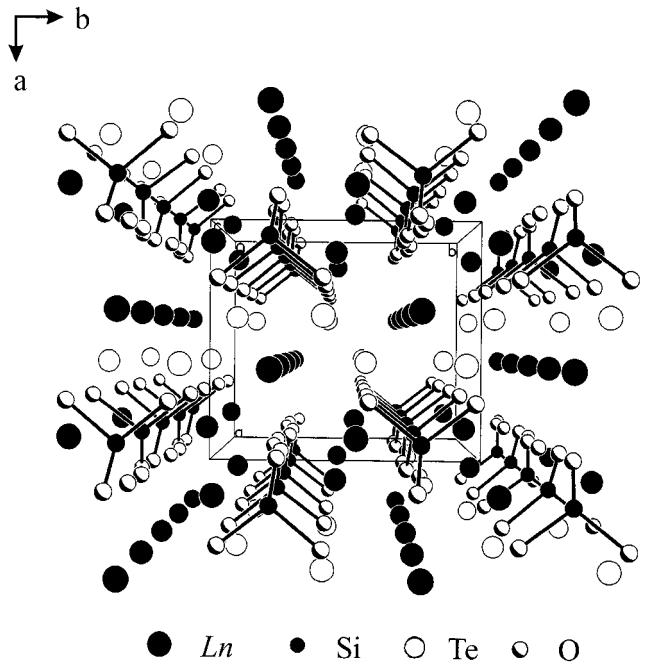

FIG. 9. Structure of orthorhombic $Ln_2(SiO_4)Te$ (Ln = Nd and Sm) as viewed down [001].

monoclinic $Pr_2(SiO_4)Te$ (26). Two consecutive $[SiO_4]^{4-}$ layers in the two structures shift in c by $2a \sin(4°)$. This shift also causes differences in the coordination of the rare-earth elements, as shown in Fig. 8.

Orthorhombic $Ln_2(SiO_4)Te$ (Ln = Nd and Sm)

These compounds are isostructural with orthorhombic $Pr_2(SiO_4)Te$ (26) and $Ln_2(SiO_4)Se$ (Ln = Sm, Dy, and Ho (4)). Their structure is shown in Fig. 9. The structure can be considered as a layered structure with $[SiO_4]^{4-}$ groups, separated by Ln^{3+} cations, extending along c and distributed nearly isotropically in the a and b directions. There are two crystallographically distinct Ln atoms: atom $Ln(1)$, located within the layer, is coordinated by six O and three Te atoms in a tricapped trigonal prism; atom $Ln(2)$, located between the layers, is coordinated by six O and two Te atoms in a dodecahedron. The silicates corrugate in the a direction, which decreases the gaps between the layers. Metrical data are presented in Table 6. The results for $Sm_2(SiO_4)Te$ are in reasonable agreement with the earlier, presumed room-temperature results (4), although the agreement is poorer than one would expect from the estimated standard deviations. In orthorhombic $Nd_2(SiO_4)Te$ the Nd–O distances range from 2.459(4) to 2.609(4) Å, which may be compared with the range of 2.2350(2) to 2.7719(6) Å in $Nd_4Mn(SiO_4)_3O$ (23). The Nd–Te distances range from 3.1565(8) to 3.3413(9) Å, compared with 3.50(1) Å in Nd_2O_2Te (27). As would be expected there is good correspondence among comparable distances in the monoclinic and orthorhombic forms of $Ln_2(SiO_4)Te$ (Ln = Nd and Sm).

TABLE 7
Colors Observed for $Ln_2(SiO_4)Te$ Compounds

$Ln_2(SiO_4)Te$	Monoclinic ($P2_1/c$)	Orthorhombic ($Pbcm$)
$Nd_2(SiO_4)Te$	Yellow	Light purple
$Sm_2(SiO_4)Te$	Vivid red	Dark red[b]
$Pr_2(SiO_4)Te$[a]	Light green	Light green

[a] Reference (26).
[b] Described as "black" in Ref. (4).

$Ln_2(SiO_4)Te$ Colors

The colors observed visually for this class of compounds are listed in Table 7. Although the electronic structure of the rare-earth element partly accounts for the observed differ-

TABLE 6
Bond Lengths (Å) and Selected Bond Angles (°) for Orthorhombic $Ln_2(SiO_4)Te$ (Ln = Nd and Sm)

$Nd_2(SiO_4)Te$				$Sm_2(SiO_4)Te$			
Bond length (Å)		Bond angle (°)		Bond length (Å)		Bond angle (°)	
Nd(1)–O(1) × 2	2.459(4)	O(2)–Si(1)–O(2)	106.5(3)	Sm(1)–O(1) × 2	2.431(4)	O(2)–Si(1)–O(2)	106.4(3)
Nd(1)–O(1) × 2	2.484(4)	O(2)–Si(1)–O(1) × 2	104.2(2)	Sm(1)–O(1) × 2	2.446(4)	O(2)–Si(1)–O(1) × 2	103.9(2)
Nd(1)–O(2) × 2	2.609(4)	O(2)–Si(1)–O(1) × 2	119.7(2)	Sm(1)–O(2) × 2	2.591(4)	O(2)–Si(1)–O(1) × 2	119.9(2)
Nd(1)–Te(1)	3.1565(8)	O(1)–Si(1)–O(1)	103.5(3)	Sm(1)–Te(1)	3.1175(8)	O(1)–Si(1)–O(1)	103.8(3)
Nd(1)–Te(1)	3.3046(8)			Sm(1)–Te(1)	3.2443(8)		
Nd(1)–Te(1)	3.3413(9)			Sm(1)–Te(1)	3.3119(8)		
Nd(2)–O(1) × 2	2.496(4)			Sm(2)–O(1) × 2	2.468(4)		
Nd(2)–O(2) × 2	2.496(4)			Sm(2)–O(2) × 2	2.449(4)		
Nd(2)–O(2) × 2	2.515(4)			Sm(2)–O(2) × 2	2.481(4)		
Nd(2)–Te(1) × 2	3.3203(6)			Sm(2)–Te(1) × 2	3.2723(6)		
Si(1)–O(2) × 2	1.633(4)			Si(1)–O(2) × 2	1.625(4)		
Si(1)–O(1) × 2	1.650(4)			Si(1)–O(1) × 2	1.641(4)		

ences in colors, changes in coordination geometry are clearly responsible for the differences in the Nd and Sm dimorphic pairs.

ACKNOWLEDGMENTS

This work made use of facilities supported by the MRSEC program of the National Science Foundation (DMR96-32472) at the Materials Research Center of Northwestern University. This research was supported by the National Science Foundation through Grant DMR 97-09351.

REFERENCES

1. K. Stöwe, *Z. Naturforsch., B: Anorg. Chem., Org. Chem.* **49,** 733–740 (1994).
2. C. Deudon, A. Meerschaut, and J. Rouxel, *J. Solid State Chem.* **104,** 282–288 (1993).
3. T. D. Brennan and J. A. Ibers, *Acta Crystallogr., Sect. C: Cryst. Struct. Commun.* **47,** 1062–1064 (1991).
4. H. Person, M. Grupe, and W. Urland, *Z. Anorg. Allg. Chem.* **626**, 280–283 (2000).
5. J. C. Huffman and W. E. Streib, unpublished work, 1990.
6. SMART Version 5.054 Data Collection and SAINT-Plus Version 6.02A Data Processing Software for the SMART System, Bruker Analytical X-Ray Instruments, Inc., Madison, WI, 2000.
7. G. M. Sheldrick, SHELXTL DOS/Windows/NT Version 5.10, Bruker Analytical X-Ray Instruments, Inc., Madison, WI, 1997.
8. Y. Le Page, *J. Appl. Crystallogr.* **20,** 264–269 (1987).
9. D. de Saint-Giniez, P. Laruelle, and J. Flahaut, *C. R. Seances Acad. Sci., Ser. C* **267,** 1029–1032 (1968).
10. J. Flahaut, *in* "Handbook on the Physics and Chemistry of Rare Earths" (K. A. Gschneidner, Jr., and L. R. Eyring, Eds.), Vol. 4, pp. 1–88, North-Holland, New York, 1979.
11. A. A. Eliseev and G. M. Kuzmichyeva, *in* "Handbook on the Physics and Chemistry of Rare Earths" K. A. Gschneidner, Jr., and L. R. Eyring, Eds.), Vol. 13, pp. 191–280. North-Holland, New York, 1990.
12. B. Eisenmann, M. Jakowski, and H. Schäfer, *Mater. Res. Bull.* **19,** 77–82 (1984).
13. J. Peters and B. Krebs, *Acta Crystallogr., Sect. B: Struct. Crystallogr. Cryst. Chem.* **38,** 1270–1272 (1982).
14. R. L. Gitzendanner, C. M. Spencer, F. J. DiSalvo, M. A. Pell, and J. A. Ibers, *J. Solid State Chem.* **131,** 399–404 (1996).
15. St. Náray-Szabó, *Z. Kristallogr.* **75,** 387–398 (1930).
16. M. Mathew, I. Mayer, B. Dickens, and L. W. Schroeder, *J. Solid State Chem.* **28,** 79–95 (1979).
17. J. Felsche, *J. Solid State Chem.* **5,** 266–275 (1972).
18. C. Sieke and T. Schleid, *Z. Anorg. Allg. Chem.* **623,** 1345–1346 (1997).
19. M. Sato, Y. Kono, H. Ueda, K. Uematsu, and K. Toda, *Solid State Ionics* **83,** 249–256 (1996).
20. L. W. Schroeder and M. Mathew, *J. Solid State Chem.* **26,** 383–387 (1978).
21. N. Kalsbeek, S. Larsen, and J. G. Ronsbo, *Z. Kristallogr.* **191,** 249–263 (1990).
22. J. A. Fahey, W. J. Weber, and F. J. Rotella, *J. Solid State Chem.* **60,** 145–158 (1985).
23. E. Klüver and H. Müller-Buschbaum, *Z. Naturforsch., B: Anorg. Chem., Org. Chem.* **50,** 61–65 (1995).
24. J. Dugué, T. Vovan, and J. Villers, *Acta Crystallogr., Sect. B: Struct. Crystallogr. Cryst. Chem.* **36,** 1291–1294 (1980).
25. J. Dugué, T. Vovan, and P. Laruelle, *Acta Crystallogr., Sect. C: Cryst. Struct. Commun.* **41,** 1146–1148 (1985).
26. F. A. Weber and T. Schleid, *Z. Anorg. Allg. Chem.* **625,** 2071–2076 (1999).
27. P. M. Raccah, J. M. Longo, and H. A. Eick, *Inorg. Chem.* **6,** 1471–1473 (1967).